The 8th European Congress on Computational Methods in Applied Sciences and Engineering
ECCOMAS Congress 2022
5-–9 June 2022, Oslo, Norway

TRANSONIC BUFFET SIMULATION USING A PARTIALLY-AVERAGED NAVIER-STOKES APPROACH

ANDREA PETROCCHI[1] AND GEORGE N. BARAKOS[1]

[1] CFD Laboratory, School of Engineering
University of Glasgow, Glasgow, G128QQ, Scotland, UK

Keywords: Computational Fluid Dynamics, Transonic buffet, PANS, Turbulence modelling

Abstract. This work assesses the capability of the partially averaged Navier-Stokes (PANS) method to accurately reproduce self-sustained shock oscillations, also known as transonic buffet, occurring on supercritical aerofoils at high Reynolds numbers. Attention is paid to the comparison with unsteady Reynolds-averaged Navier Stokes (URANS) results to show the benefits of PANS, in resolving flow unsteadiness on affordable CFD grids. The role of the mesh metrics in the formulation of the PANS model is emphasized, as well as the relation of the mesh metrics with the spatiotemporal discretisation used for the numerical simulations. The aim is to extend the use of PANS to flow cases involving shock-wave boundary layer interactions to obtain accurate predictions without the need for very expensive computations.

1 INTRODUCTION

Computational fluid dynamics (CFD) has been extensively used to simulate Shock wave/boundary layer interaction (SBLI), especially at transonic conditions. Reynolds-averaged Navier Stokes (RANS) simulations have become the most popular tool in CFD because of their reduced CPU cost and wide range of applicability. Nevertheless, the prediction of SBLI phenomena with RANS simulations is not always accurate, especially when the flow is unsteady or separated. Following the increase in the availability of computational resources, direct numerical simulations (DNS) and large eddy simulations (LES) are no longer out of reach for canonical flows at moderate Reynolds numbers. Nevertheless, cases of aeronautical interest, e.g. flows around transonic wings, cannot yet be studied with such expensive methods. Therefore, in recent years, hybrid RANS/LES approaches have been introduced as a more viable option even for high Reynolds number flows.

In this context, the partially-averaged Navier-Stokes (PANS) [1] method was introduced as a bridging model between RANS and DNS. The ratios of modelled-to-total turbulent kinetic energy and dissipation, f_k and f_ϵ, respectively, are introduced to control the filter width of the turbulence simulation. When both values are equal to unity the PANS equations are identical to RANS, whereas a DNS solution is obtained when these coefficients tend to zero. The main advantage over URANS is that the resolution of a part of turbulent fluctuations is enabled, leading to an improvement in terms of predictions and greater detail of the flow structures. This feature is particularly useful for flows with separation, whether shallow or fixed-point. Buffet flows are in the former category since they exhibit an alternation of separation and reattachment. An advantage of PANS over other hybrid RANS/LES models is the potential to deliver improved results even adopting a RANS-like grid, as long as the values of the two parameters f_k and f_ϵ remain reasonably high [2]. Conversely, the switch to LES-mode of techniques like the DES

family [3] in separated flow regions, reintroduces the requirements in terms of the spatiotemporal discretisation present in LES computations, leading to a noticeable increase in CPU costs. So far, PANS simulations have been mainly tested on canonical incompressible flows. Flows around circular [4, 5] and square [6] cylinders, backward-facing steps [7], turbulent channels [8] or humps and hills [9, 10] were mostly investigated. Rare exceptions were found for transonic and supersonic flows [11, 12, 13].

Over the last two decades, there has been substantial research on transonic buffet flows, and the prediction of this phenomenon revealed to be challenging and not always accurate. For extensive coverage of the topic, the reader is referred to the review papers of Lee [14] and Giannelis et al. [15]. A number of authors [16, 17, 18] investigated the ability of URANS to capture buffet. Still, there is no consensus on the topic, and hybrid RANS/LES approaches became more popular in the analysis of the flow around two-dimensional [19, 18] and three-dimensional configurations [20]. Scale-resolving simulations were found to represent the buffet phenomenon with higher accuracy and to show significant improvements in the prediction of buffet. The main drawback of these methods is the considerably higher CPU costs stemming from the fine spatiotemporal discretisation required. Regardless, even if computations of this type can be affordable for a simplified geometry, the cost becomes prohibitive for complex 3D cases. Here rises the need for a computational approach with is accurate for the prediction of the buffet without introducing the costs of the aforementioned approaches.

In this paper, we aim at investigating the capability of PANS to predict transonic buffet around the OAT15A aerofoil [21]. Attention is paid to the efficiency of the computational method over URANS, and the capability of PANS to capture the correct flow physics at a reasonable CPU cost. The article is structured as follows: in section 2 the compressible PANS formulation is presented; in section 3 the results for the flow around the OAT15A aerofoil at both pre- and post- buffet onset are presented before drawing some conclusions in section 4.

2 MATHEMATICAL MODEL

2.1 PANS Formulation

The partially-averaged Navier-Stokes (PANS) formulation was introduced by Girimaji et al. [1] as a bridging model between RANS and DNS. This method is based on a RANS paradigm, where the blending is obtained by means of the user-prescribed unresolved-to-total ratios of turbulent kinetic energy f_k and dissipation f_ϵ, bounded between 0 and 1, acting on the turbulence closure equations. They read:

$$f_k = \frac{k_u}{k}\,, \quad f_\epsilon = \frac{\epsilon_u}{\epsilon}\,, \tag{1}$$

where u subscripts stand for unresolved and the quantities at the denominator are the total ones. The PANS method was initially derived for k-ϵ closures and then extended to the k-ω and the SST models, where f_ϵ is replaced by the unresolved-to-total turbulence frequency $f_\omega = f_\epsilon / f_k$. These formulations inherit from the parent RANS models an eddy viscosity based on a Boussinesq approximation, that is reduced with respect to the RANS case because of the effect of the f_k parameter: since only a fraction of the turbulent kinetic energy is modelled, the corresponding value of the eddy viscosity is reduced.

In this work, the SST-PANS formulation is adopted. It reads

$$\frac{\partial\left(\rho k\right)}{\partial t} + \frac{\partial\left(\rho U_j k\right)}{\partial x_j} = P_k - \beta^* \rho k \omega + \frac{\partial}{\partial x_j}\left[\left(\mu + \mu_t \sigma_k \frac{f_\omega}{f_k}\right)\frac{\partial k}{\partial x_j}\right], \tag{2}$$

$$\frac{\partial(\rho\omega)}{\partial t}+\frac{\partial(\rho U_j\omega)}{\partial x_j}=\frac{\gamma}{\nu_t}P_k-\beta'\rho\omega^2+\frac{\partial}{\partial x_j}\left[\left(\mu+\mu_t\sigma_\omega\frac{f_\omega}{f_k}\right)\frac{\partial\omega}{\partial x_j}\right]+2\frac{f_\omega}{f_k}(1-F_1)\frac{\rho\sigma_{\omega2}}{\omega}\frac{\partial k}{\partial x_j}\frac{\partial\omega}{\partial x_j}, \tag{3}$$

where ρ is the density, U_j is the flow velocity, μ is the dynamic molecular viscosity and μ_t is the turbulent viscosity. Here, the turbulent kinetic energy k and frequency ω are the modelled fractions and the u subscripts were dropped for sake of simplicity. In the ω-equation, $\beta'=\left(\gamma\beta^*-\frac{\gamma\beta^*}{f_\omega}+\frac{\beta}{f_\omega}\right)$; F_1 is the SST blending function while $\gamma,\beta,\beta*,\sigma_k,\sigma_\omega$ are the model coefficients [22]. The turbulent viscosity is calculated as in the reference [22].

A debated point is how to prescribe the value of f_k. Three main approaches can be distinguished: **Constant**, f_k is fixed in space and time; **Static**, f_k follows an optimal spatial distribution found after a preliminary RANS simulation; **Dynamic**, f_k is a function of space and time. There is no consensus on which of these three approaches should be used; the constant approach is preferred by its advocates because no commutation errors are introduced adopting a spatially and temporally constant filter, although an *a priori* calibration is required. A variable approach is preferred in flows where confined regions of high turbulent content and anisotropies in the grid are present since a variable filter allows an optimal usage of resources by adapting to both the local turbulent content and the grid size. The dynamic approach introduces some additional CPU costs over the static and constant approaches due to the dynamic evaluation of f_k. Therefore, a static approach is more suitable to problems with localised statistically steady turbulence, whereas the dynamic approach is required where coming to intrinsically unsteady flows like for the case of buffet flows and hence is adopted in this work. The estimate adopted in this work is:

$$f_k=C_{\mathrm{PANS}}\left(\frac{\Delta}{L_t}\right)^{2/3}, \tag{4}$$

where $L_t=\sqrt{k}/(C_\mu\omega)$ it the local turbulent length scale, Δ is the local grid size and C_{PANS} is a model constant. The f_ϵ parameter is usually set to one, under the assumption that all dissipative scales are not resolved in the computation. This approach is suitable for high Reynolds numbers for which there is a net separation between energy-containing and dissipative scales [1].

2.2 HMB3 Solver

The PANS method was implemented in the helicopter multi-block (HMB) solver of the University of Glasgow [23], a three-dimensional, fully implicit, structured, multi-block code for the solution of the Navier-Stokes equations. The Navier-Stokes equations are discretised using a cell-centred finite volume approach. The computational domain is divided into a finite number of non-overlapping control volumes, and the governing equations are applied to each cell. Also, the Navier- Stokes equations are re-written in a curvilinear co-ordinate system which simplifies the formulation of the discretised terms since body-conforming grids are adopted here. The spatial discretisation of the equations leads to a set of ordinary differential equations in time,

$$\frac{d}{dt}(\mathbf{W}_{ijk}V_{ijk})=-\mathbf{R}_{ijk}(\mathbf{W}), \tag{5}$$

where $\mathbf{W}$ and $\mathbf{R}$ are the vectors of cell conserved variables and residuals respectively. The convective terms are discretised using the Osher's upwind scheme. MUSCL variable extrapolation is used to provide second-order accuracy with the Van Albada limiter to prevent spurious

oscillations around shock waves. The integration in time of the previous equation to a steady-state solution is performed using an implicit time-marching scheme. The linearized system of equations is solved using the generalized conjugate gradient method with a block incomplete lower–upper (BILU) factorization as a pre-conditioner. The solver offers several one-equation, two-equation, three-equation, and four-equation turbulence models. LES, DES, delayed DES (DDES), improved DDES (IDDES), SAS and PANS methods are also available.

3 APPLICATION OF PANS TO BUFFET

3.1 Description of the employed test case

In the present study, the flow around the supercritical aerofoil OAT15A is investigated. This configuration was studied [21] in the S3Ch wind tunnel at ONERA. The wing section had a chord of $c = 0.23$m and a span of 0.78 m, a thickness-to-chord ratio of $t/c = 0.123$, and a trailing edge thickness-to-chord of 0.005. The wing was mounted in a squared section wind tunnel having nominal dimensions of 0.78m $\times$ 0.78m $\times$ 2.2m. An adaptation technique was adopted at the lower and upper walls to reproduce free-stream conditions. Measurements were collected at free-stream Mach numbers of 0.7-0.75, chord-based Reynolds number of $\mathrm{Re}_c = 3 \times 10^6$, and angles of attack of 1.36 - 3.9 deg. Static and dynamic pressure measurements in the vicinity of the mid-span section allowed the detection of the flow unsteadiness at an angle of attack of 3.1 deg, culminating in a self-sustained shock-induced oscillation at higher angles. At M = 0.73 and $\alpha = 3.5$ deg, a laser Doppler velocimetry (LDV) system was also employed. These measurements were complemented with oil-flow and schlieren visualisations.

Here, the study is focused on two different flow conditions, at M = 0.73 and angles of attack of $\alpha = 2.5$, 3.5 deg, representative of a statistically steady flow, a fully-established buffet flow, respectively.

3.2 CFD grids and numerical setup

The three-dimensional flow domain (3D in table 2) consists of half of the wind tunnel used in the experimental campaign and it is sketched in fig. 1. The grids adopted for this configuration are indicated as C3 and M3 in table 1. At the inflow, free stream values of the pressure, density

Table 1: Main features of the different grids used for computations.

Grid #	$N_{aerofoil}$	N_z	$\Delta z_{wall}/c$	$\Delta z_{max}/c$	N_y	$\Delta n_{aerofoil}/c$	$\Delta z_{walls}/c$	N_{wake}	$\Delta x_{TE}/c$	N_{tot}
C2	470	30	-	0.0083	115	5×10^{-6}	-	220	5×10^{-6}	4.19×10^6
F2	710	60	-	0.0042	115	5×10^{-6}	-	220	5×10^{-6}	9.07×10^6
C3	405	76	2×10^{-6}	0.033	102	5×10^{-6}	5×10^{-3}	87	5×10^{-6}	$\simeq 5.03 \times 10^6$
M3	510	164	2×10^{-6}	0.015	102	5×10^{-6}	5×10^{-3}	151	5×10^{-6}	$\simeq 16.70 \times 10^6$

and velocity are imposed, while adiabatic wall conditions were imposed on both the aerofoil and the tunnel sidewall, since no detail was given on the sidewall treatment of the boundary layer. The symmetry boundary conditions imposed at the centre plane allowed simulating just half of the domain. The upper and lower walls were modelled as slip-walls, and the shape was extracted from a preliminary 2D RANS simulation to replicate the results of the adaptive technique used in the experimental campaign. At the outlet, the tunnel back pressure was imposed in the subsonic region. Computations on an unconfined configuration with reduced spanwise extent ($L_z = 0.25c$) were also performed (2D in table 2, C2 and F2 in table 1).

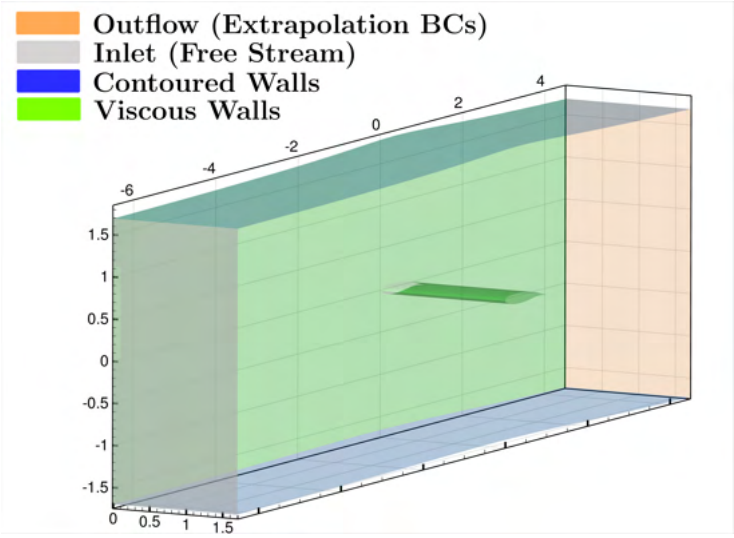

Figure 1: Computational domain with coloured by boundary conditions. The symmetry plane at $z/c = 1.7$ is not coloured.

3.3 Pre-buffet flow

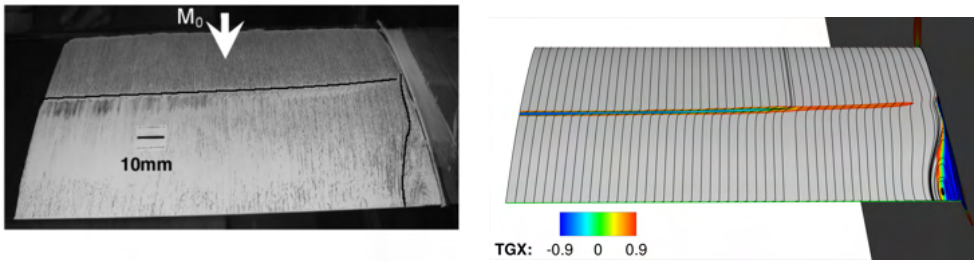

Figure 2: Left: oil flow visualization around the OAT15A [21] at $\alpha = 2.5$ deg (shock position and separation line marked with a solid, black line); right: friction lines from CFD. The surface is coloured by the streamwise component of $\dfrac{\partial \mathbf{u}}{\partial \mathbf{n}}$, i.e the spatial derivative of the velocity field in the direction normal to the wall.

Fig. 2 underlines the effect of the wind tunnel walls. The shock position can be detected by the negative values of the streamwise component of $\dfrac{\partial \mathbf{u}}{\partial \mathbf{n}}$ at the surface and, going towards the sidewall, from a sudden deflection of the friction lines. The shock curves when approaching the sidewalls, and a region of separated flow is confined within the 10% of the span, in agreement with the experimental results.

Moreover, because of the viscous sidewall, the turbulence level in the boundary layer grows as it approaches the aerofoil. This coincides with a growth in the turbulence length scales and a following reduction in f_k at the wall. Although the behaviour of the method is correct, this introduces the need for an overly fine spatial and temporal distribution in a region of limited interest for the development of transonic buffet. Therefore, in this work, an f_k value of 1

Table 2: Computations performed at different angles of attack, on different grids, and using different timesteps. All computations were run at $M_\infty = 0.73$. In the run ID, U stands for URANS while P for PANS.

Run #	α	**2D/3D**	**Mesh**	C_{PANS}	Δt	$\langle C_l \rangle$	St
Exp.	-	-	-	-	-	$\simeq 0.875$	-
U1	2.5	3D	Coarse	-	0.1	0.874	
P1	2.5	3D	Coarse	3.3	0.1	0.879	
P1.1	2.5	3D	Coarse	1.0	0.1	0.841	
P1.2	2.5	3D	Coarse	0.5	0.1	0.733	
Exp.	-	-	-	-	-	$\simeq 0.875$	0.066
U4	3.5	3D	Coarse	-	0.01	0.82	-
P4	3.5	3D	Coarse	1.0	0.01	0.833	0.042
P4.1	3.5	3D	Coarse	0.5 & clip 0.2	0.01	0.746	0.043
P4.2	3.5	3D	Coarse	0.5 & clip 0.4	0.01	0.739	0.046
P4.4	3.5	3D	Coarse	0.5 & clip 0.6	0.01	0.835	-
P6	3.5	3D	Medium	0.5	0.005	0.733	
P7	3.5	2D	Fine	0.5	0.005	0.748	0.065

was imposed within a distance of 0.15c from the wall. This URANS region encompasses the separation region at the wing-wall junction throughout the buffet period. Since the vortices in the detached region at the walls were deemed to be steady in the experiments, the approach has been used.

Practically, identical C_p distributions were obtained with different PANS coefficients and in good agreement with the experimental results.

3.4 Buffet Simulation

Here the results from the simulations performed at $\alpha = 3.5$ deg are shown. Fig. 3 shows the lift coefficient history for the simulations (U4, P4-P4.2) on the coarser grid C3. The grid

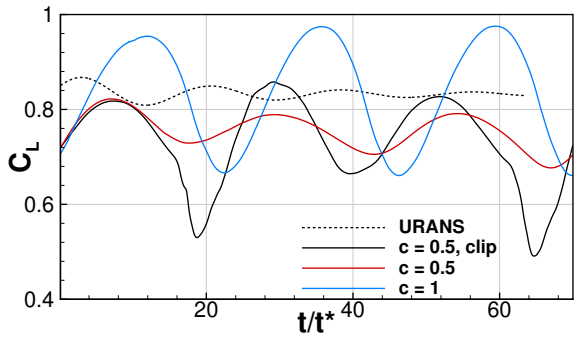

Figure 3: Temporal evolution of the lift coefficient around the OAT15A at $\alpha = 3.5$.

under analysis (details in table 1) is rather coarse in the spanwise direction presenting the features of usual RANS grids. Even at this condition, the usage of PANS led to benefits in the prediction of transonic buffet. The URANS simulation converged to a steady-state after about

ten travel times, while the PANS ones are able to predict the buffet. In the former case, the corner separation induced a spanwise flow deviation at the trailing edge preventing the flow from separating. Even if the flow separated at the shock foot, the separation region did not merge with the one at the trailing edge and the buffet was inhibited. The main reasons can be found in an excessive flow separation at the corner, together with a too high level of eddy viscosity given from the URANS in the post-shock region. Therefore, the presence of the tunnel walls does not help the developing of the self-sustained shock oscillation. Conversely, the PANS simulation predicts the buffet developing according to a precise pattern, shown in fig. 4. Approaching

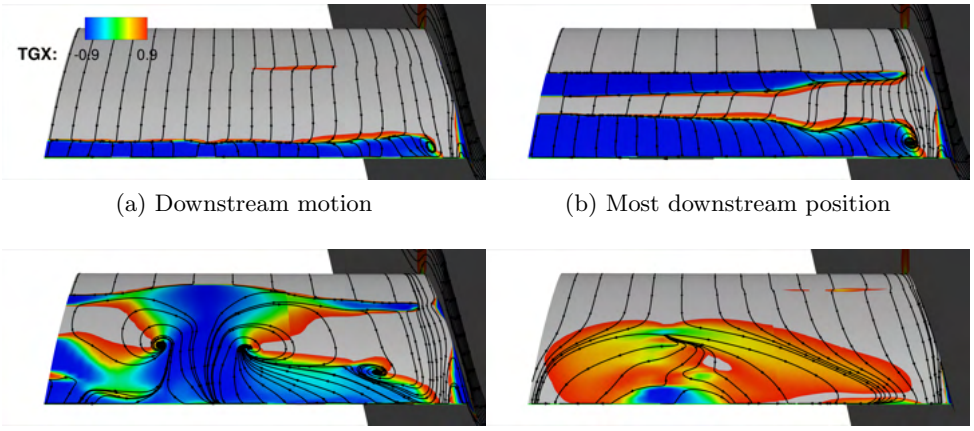

(a) Downstream motion (b) Most downstream position

(c) Upstream motion (d) Most upstream position

Figure 4: Surface friction lines at different phases of the buffet period. Results from simulation P4.2 in table 2.

the most downstream position (a), the flow is attached and the shock strength increases until the flow separates underneath; at the same time, trailing edge separation occurs (b). The two regions merge around the centerline inducing a flow acceleration between the corner and central separated regions. The effect of this is a size decrease in the corner separation and the creation of vortical structures at the boundary with the central separated flow. When the flow is fully separated after the shock, this is affected by the disturbances coming from the trailing edge and the shock begins to move upstream. In parallel, the aforementioned vortical structures propagate in the separated region and extend to the entire wingspan giving rise to a region characterized by large stall cells (c), in agreement with what observed in the experiments [21]. A comparison between the computational and experimental results is given in fig. 5. Approaching the most upstream position, the shock strength decreases, the flow reattaches completely (d), and a new oscillation begins with the shock moving downstream.

The computations on the unconfined configuration, not shown here, did not present such a three-dimensional development of buffet. Indeed, the reduced spanwise extent and the absence of the viscous walls resulted in 2D buffet behaviour, only displaying the alternated boundary-layer separation and reattachment and a straight shock front.

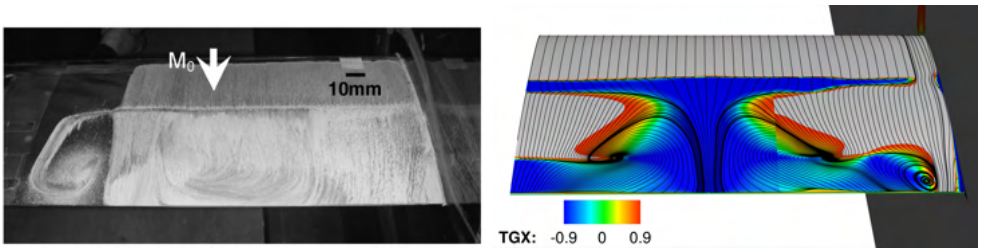

Figure 5: Left: oil flow visualization around the OAT15A (picture taken from [21]) at $\alpha = 3.5$ deg; right: friction lines from CFD. Results from simulation P4.2 in table 2.

3.4.1 Influence of C_{PANS}

Here, the influence of the C_{PANS} coefficient and of the f_k are investigated. Adopting the estimate of eq. (4), the value of f_k tends toward the zero in the separated region, and, therefore, the parameter must be clipped to a suitable value to prevent an excessive reduction of the eddy viscosity. Fig. 3 shows the time evolution of the aerodynamic coefficients for two values of C_{PANS}. For $C_{\text{PANS}} = 0.5$, two different values of the clip are used. In the case of $C_{\text{PANS}} = 1$ the oscillations are regular, while in the case of $C_{\text{PANS}} = 0.5$ the oscillations become irregular. In the latter case, the mean value of the lift coefficient decreases as well as the mean amplitude of oscillation, and the same behaviour was found for the other aerodynamic coefficients, not shown here. This is reflected in the pressure coefficient and fluctuations on the aerofoil, shown in fig. 6. The pressure coefficient distribution and RMS value were evaluated, averaging the pressure signal extracted at probes located at the same locations of the pressure sensors used in the experiments. A wider oscillation coincides with a higher pressure RMS, while in the case of $C_{\text{PANS}} = 0.5$ the shock excursion was smaller, as well as the peak RMS. Conversely, the higher the C_{PANS} the lower C_p is. In both cases, the RMS at the trailing edge was underestimated. Fig. 7 complements the previous figure adding some more insight. In the case of $C_{\text{PANS}} = 1$ the

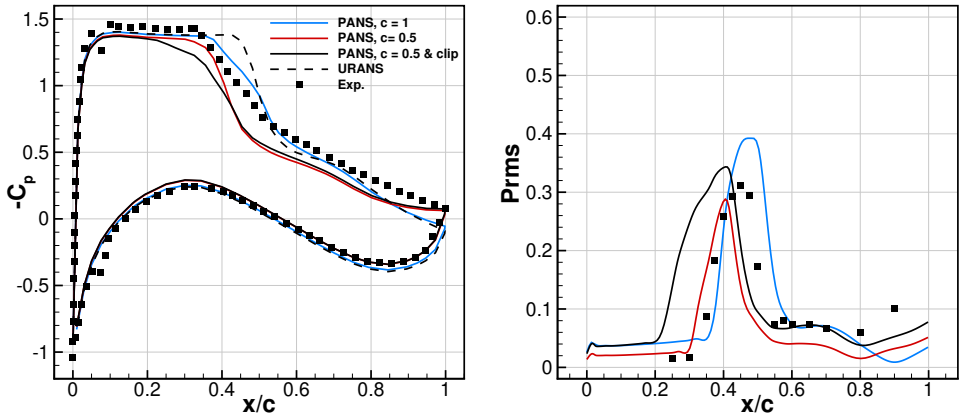

Figure 6: Left: time-averaged pressure coefficient at $\alpha = 3.5$ deg; right: root means square of the pressure. Experiments from [21].

separation was incipient at both the trailing edge and at the shock foot. The two recirculation regions were generated at the most downstream shock position, but they did not merge in a

unique separation bubble. Conversely, the lower eddy viscosity obtained by lowering the PANS parameter allows for the flow separation at the trailing edge during a great part of the shock oscillation. The separated region at the shock foot is generated when the shock approaches its most downstream position and merges with the other separation region, giving rise to a single separation bubble. Nevertheless, the formation of the two recirculation zones should occur almost at the same time, as shown in [18], e.g., suggesting that the trailing edge eddy viscosity level is too low. This in turn reflects in a too upstream average shock position. From fig. 7, a different behaviour at the sidewall is found to influence the buffet dynamics. In the first case ($C_{\text{PANS}} = 1$), a much wider separation region is present at the corner. The blockage effect delays the trailing edge separation, that cannot catch up with the shock foot separation. Moreover, the corner separation changes in size over the buffet period and influences the shock position at the centre plane. The opposite happens when $C_{\text{PANS}} = 0.5$ is adopted. The excessive separation at the centre plane, where PANS is active, forces the flow to bend towards the wall, causing a decrease in the corner separation size. This reflects in an almost straight shock front. In addition, the vortical structures generated in the recirculation region on the wall can propagate towards the symmetry plane in the separated boundary layer extending throughout the wingspan. When

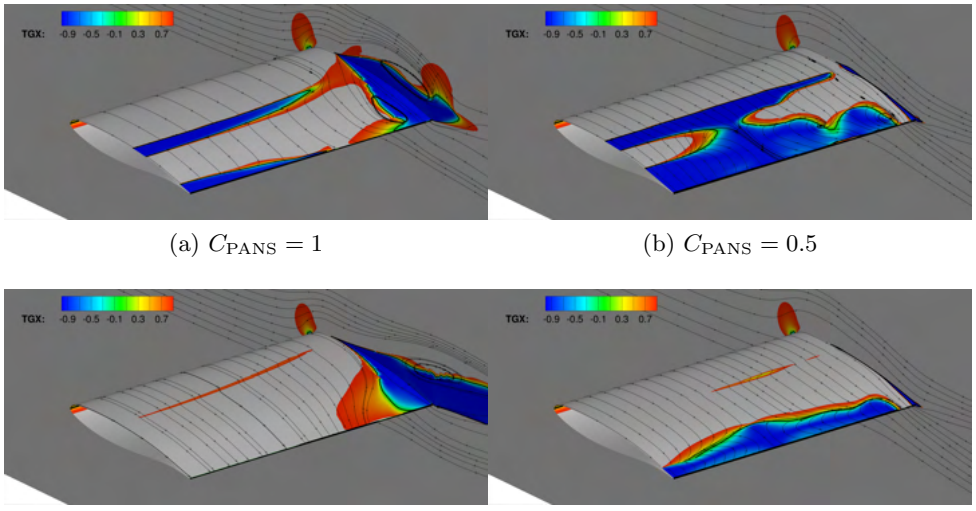

(a) $C_{\text{PANS}} = 1$ (b) $C_{\text{PANS}} = 0.5$

(c) $C_{\text{PANS}} = 1$ (d) $C_{\text{PANS}} = 0.5$

Figure 7: Friction lines over the aerofoil surface. The black line marks the reversed flow region.

clipping f_k to a higher value (P4.1), the eddy viscosity level at the TE increased and the flow was less prone to separation over the buffet period. This reflected in an effective alternation of attached and separated boundary layer that, in turn, caused the shock oscillation to be wider and the RMS value at the trailing edge to improve. Nevertheless, an average upstream position is still predicted. Increasing again the value of the clip ($f_{k,inf} = 0.6$) led to a failure in predicting the self-sustained oscillations. Therefore, the adopted estimate for the f_k parameter was found to be sensitive to both parameters investigated. Nonetheless, when set properly, the computations were able to predict the right physics and provided a good comparison with the experiments.

Table 3: Comparison between computational times of PANS and URANS. ABAH: apply boundary and halo; IATS: initialize and time step; CHOG: calculate high order gradients; CRJ: calculate residual Jacobian; CP: calculate preconditioner; SLS: solve linear system.

	GCG iter.	**ABAH [s]**	**IATS [s]**	**CHOG [s]**	**CRJ [s]**	**CP [s]**	**SLS[s]**	**Tot**
URANS	3.86	0.31	0.055	0.00024	0.65	0.09	0.83	**1.95**
PANS	4.59	0.31 (+1%)	0.055 (-1 %)	0.00025 (+8 %)	0.70 (+7 %)	0.09 (-3 %)	0.85 (+2 %)	**2.00 (+3.1%)**

3.5 Computational performance and cost

Tab. 3 presents the CPU cost associated with PANS and URANS simulations. The comparison was over one characteristic time, i.e. over 100 computational timesteps. In the analysis, the same grid and the same number of processors were used. Since URANS tends to a steady solution while the PANS describes an intrinsically unsteady flow, the number of inner iterations required to meet the convergence criterion on the flow residual is different; therefore, the averages were taken over the number of inner iterations of the implicit dual-time stepping scheme. This was done to identify the net additional cost of the PANS routine in the CFD solver. From the table, it can be seen that the higher increase is that on the evaluation of the residual Jacobian, where the PANS routines are modifying the source terms of the k and ω equations. Moreover, the number of iterations of the GCG scheme for the solution of the linear scheme is slightly increased. This reflects in an increase in the total computational time of about 3% when compared to URANS. The ability of PANS to work in URANS-mode in agreement with the grid capability to resolve structures was shown.

4 CONCLUSIONS

In this work, the application of PANS for the flow around the OAT15A section was presented. Computations on confined and unconfined configurations were carried out since the wind tunnel presence influenced the buffet dynamics by introducing a strong three-dimensionality to the flow. At pre-buffet conditions, the presence of the wind tunnel walls resulted in an irregular shock front and a region of separated flow at the wing-wall junction. At pre-buffet condition, the PANS approach recovered the URANS behaviour, given a reasonable distribution of the f_k parameter. In order to avoid the costs associated with the PANS approach at the wall, where a high level of turbulence develops in the boundary layer, the transition from RANS to PANS was fixed at $0.15c$ from the sidewall. After the onset, although the buffet mechanism maintained its two-dimensional nature, the interaction with the separated region at the wall-wing junction was shown to be crucial in the generation of a pair of cells at the mid-span of the wing. Conversely, the unconfined configuration showed a typical two-dimensional behaviour with an alternated separation and reattachment of the flow on the suction side of the aerofoil. In both cases, the k-ω SST model was not able to predict the buffet although the angle of attack was well beyond the buffet onset, while the use of PANS unlocked the shock oscillations. The flow physics is captured correctly, with the unsteady loads exhibiting slightly aperiodic oscillations.

The role of f_k in the PANS formulation was crucial. High values of f_k did not reduce enough the eddy viscosity to unlock the trailing edge separation and an increased size of the separation region at the corner was found. The bubble pulsation induced a shock oscillation all over the wingspan. In that case, there was no presence of 3D vortical structures. A reduced value of f_k, corresponding to $C_{\mathrm{PANS}} = 0.5$ in this case, allowed to predict the correct flow topology, with

the trailing edge separation that, developing, acted to reduce the size of the corner separation. The formation of a separation region, spanning from the shock foot to the trailing edge, was detected in this case. Within this region, large three-dimensional structures developed and propagated from the sidewall to the symmetry plane. Additional care must be taken in clipping the f_k to a minimum value according to the grid resolution. Although the agreement with the experiments [21] is not perfect (buffet frequency and shock position are slightly mispredicted), the flow exhibits the correct physical behaviour, as shown in figs. 2 and 5. The average quantities are in fair agreement with experiments. Moreover, the PANS approach proved to be helpful even at URANS resolution, at little additional expense ($\simeq 3\%$). PANS is applicable for large scale simulations and provides enhanced results with respect to URANS.

Future efforts will be devoted on the application of this technique to flows with SBLI, paying attention to the corner flow behaviour, which in this work proved to be troublesome. Moreover, a different estimate of the f_k parameter accounting for the local grid and flow features will be pursued to avoid the preliminary calibration of the method, so far necessary.

REFERENCES

[1] S.S. Girimaji and K.S. Abdol-Hamid, Partially-averaged Navier Stokes model for turbulence: implementation and validation. *AIAA Aerospace Sciences Meeting and Exhibit* (2005). Reno, NE, USA.

[2] D. Luo, Numerical simulation of turbulent flow over a backward facing step using partially averaged Navier-Stokes method. *Journal of Mechanical Science and Technology* (2019). **33**:2137–2148.

[3] P.R. Spalart, W.H. Jou, M. Strelets and S.R. Allmaras, Comments on the Feasibility of LES for Wings, and on a Hybrid RANS/LES Approach. *Advances in DNS/LES: Direct numerical simulation and large eddy simulation* (1997). Reno, NE, USA.

[4] K.S. Abdol-Hamid and S.S. Girimaji, A Two-Stage Procedure Toward the Efficient Implementation of PANS and Other Hybrid Turbulence Models. *National Aeronautics and Space Administration, NASA/TM-2004-213260* (2004).

[5] F.S. Pereira, G. Vaz, L. Eca and S.S. Girimaji, Simulation of the flow around a circular cylinder at Re=3900 with Partially-Averaged Navier-Stokes equations. *International Journal of Heat and Fluid Flow* (2018). **69**:234–246.

[6] B. Basara, Z. Pavlovic and S.S. Girimaji, A new approach for the calculation of the cut-off resolution parameter in bridging methods for turbulent flow simulation. *International Journal of Heat and Fluid Flow* (2018). **74**:76–88.

[7] A. Frendi, A. Tosh and S.S. Girimaji, Flow Past a Backward-Facing Step: Comparison of PANS, DES and URANS Results with Experiments. *International Journal for Computational Methods in Engineering Science and Mechanics* (2007). **8**:23–28.

[8] B Basara, S. Krajnovic, S. Girimaji and Z. Pavlovic, Near-Wall Formulation of the Partially Averaged Navier–Stokes Turbulence Model-Layer Interaction. *AIAA Journal* (2011). **49**:2627–2636.

[9] L. Davidson and C. Friess, A new formulation of f_k for the PANS model. *Journal of Turbulence* (2019). **20**:322–336.

[10] C. Friess and L. Davidson, A formulation of PANS capable of mimicking IDDES. *International Journal of Heat and Fluid Flow* (2020). **86**:1–25.

[11] D. Basu, A. Hamed and K. Dias, Assessment of partially averaged Navier/Stokes (PANS) multiscale model in transonic turbulent separated flows. *ASME/AJME 2007 5th Joint Fluids Engineering Conference* (2007). San Diego, CA, USA.

[12] D. Luo, C. Yan and X. Wang, Computational study of supersonic turbulent-separated flows using partially averaged Navier-stokes method. *Acta Astronautica* (2015). **107**:234–246.

[13] V. Bonnifet, G.A. Gerolymos and I. Vallet, Transonic Buffet Prediction using Partially Averaged Navier-Stokes. *23rd AIAA Computational Fluid Dynamics Conference* (2017). Denver, CO, USA.

[14] B.H.K. Lee, Self-sustained shock oscillations on airfoils at transonic speeds. *Progress in Aerospace Sciences* (2001). **37**:147–196.

[15] N.F. Giannelis, G.A. Vio and O. Levinski, A review of recent developments in the understanding of transonic shock buffet. *Progress in Aerospace Sciences* (2017). **92**:39–84.

[16] G. Barakos and D. Drikakis, Numerical simulation of transonic buffet fow using various turbulence closures. *International Journal of Heat and Fluid Flow* (2000). **21**:620–626.

[17] E. Goncalves and R. Houdeville, Turbulence model and numerical scheme assessment for buffet computations. *International Journal for Numerical Methods in Fluids* (2004). **46**:1127–1152.

[18] F. Grossi, M. Braza and Y. Hoarau, Prediction of Transonic Buffet by Delayed Detached-Eddy Simulation. *AIAA Journal* (2014). **52**:2300–2312.

[19] S. Deck, Numerical Simulation of Transonic Buffet over a Supercritical Airfoil. *AIAA Journal* (2005). **43**:1556-1566.

[20] L. Masini, S. Timme and A. J. Pace, Scale-Resolving Simulations of a Civil Aircraft Wing Transonic Shock-Buffet Experiment. *AIAA Journal* (2020). **58**:4322–4338.

[21] L. Jacquin, P. Molton, S. Deck, B. Maury and D. Soulevant, Experimental study of shock oscillation over a transonic supercritical profile. *AIAA Journal* (2009). **47**:1985–1994.

[22] F.R. Menter, Two-equation eddy-viscosity turbulence models for engineering applications. *AIAA Journal* (1994). **32**:1598–1605.

[23] R. Steijl, G. Barakos and K. Badcock, A framework for CFD analysis of helicopter rotors in hover and forward flight. *International Journal for Numerical Methods in Fluids* (2006). **51**:819–847.